J. Plasma Phys. (2024), *vol*. 90, 905900208 © The Author(s), 2024.
Published by Cambridge University Press
doi:10.1017/S0022377824000394

Study of the pellet ablation cloud using the tomography technique for two-directional simultaneous photography in GAMMA 10/PDX

M. Yoshikawa [1],†, Y. Nakashima [1], J. Kohagura [1], Y. Shima [1], S. Kobayashi [2], R. Minami [1], N. Ezumi [1] and M. Sakamoto [1]

[1]Plasma Research Center, University of Tsukuba, Tsukuba 305-8577, Japan

[2]Institute of Advanced Energy, Kyoto University, Uji 611-0011, Japan

(Received 17 December 2023; revised 8 March 2024; accepted 8 March 2024)

The pellet ablation mechanism is an interesting subject for plasma fuelling in fusion plasmas. In GAMMA 10/PDX, pellet injection experiments for higher density plasma production are planned to conduct detached plasma experiments in the higher density plasma condition. We measured the pellet ablation cloud by using the two-directional simultaneous photography system in GAMMA 10/PDX. The tomography reconstruction technique was used for considering the pellet trajectory in the plasma and pellet ablation. The three-dimensional pellet trajectory and pellet ablation images in the plasma were clearly obtained for the first time, to the best of our knowledge.

Keywords: pellet ablation cloud, two-directional, high-speed camera, GAMMA 10/PDX

1. Introduction

Pellet fuelling is a useful method for particle fuelling in the core region of fusion plasmas (Combs *et al.* 1985; Kawamori *et al.* 2000; Sakamoto *et al.* 2004; Kubota *et al.* 2007; Baldzuhn *et al.* 2019; Baylor *et al.* 2021; Yoshikawa *et al.* 2022). The study of the mechanisms of ablation cloud formation around a pellet interacting with the background plasma is an important subject. Temporally and spatially resolved imaging observations are useful for studying pellet ablation in plasma. In many fusion devices, radiation intensity profiles from ablation clouds have been observed using high-speed camera systems and Hα line emission measuring array systems. We prepared a two-directional simultaneous photography (TDSP) system consisting of a two-to-one optical fibre and a high-speed camera system, and constructed an analysis method using the tomography technique for pellet ablation study.

We successfully simulated the detached plasma formation by injecting additional neutral gas into the D-module (Nakashima *et al.* 2015; Yoshikawa *et al.* 2021). The density of the core plasma was lower than that of the SOL plasma of normal fusion devices. To study the mechanisms of detached plasma formation in the higher plasma density region, we plan to perform pellet injection into the central cell plasma to increase the core plasma density. Pellet ablation studies are also important for understanding the pellet fuelling mechanisms.

† Email address for correspondence: yosikawa@prc.tsukuba.ac.jp

The pellet ablation cloud and pellet trajectory in the plasma must be directly observed to study pellet ablation mechanisms.

In this study, we present a TDSP system and its application to pellet ablation measurements in the tandem mirror GAMMA 10/PDX. Moreover, we present, for the first time to the best of our knowledge, a reconstructed three-dimensional (3-D) image of the pellet ablation cloud using the algebraic reconstruction technique (ART) for tomography.

2. Experimental apparatus

2.1. *GAMMA 10/PDX*

GAMMA 10/PDX is the largest tandem mirror device consisting of the main confining region of the central cell, two axisymmetric minimum-B anchor cells, and two plug and barrier cells. In the west-end region, the divertor simulation experimental module (D-module) was set for divertor simulation experiments with the use of the end-loss plasma from the core plasma. The x-axis and y-axis are defined perpendicular to the magnetic field in the vertical and horizontal directions, respectively, and the z-axis is parallel to the magnetic field. The mid-plane is $z = 0$ m. The plasma is produced and maintained with the application of ion cyclotron resonance frequency (ICRF) wave heating after the initial plasma injection by the plasma gun. The electron density radial profile is measured by using a multichannel microwave interferometer system set at $z = 0$ m (Yoshikawa *et al.* 2018). Typical electron densities and temperatures are approximately 2×10^{12} cm^{-3} and 25 eV in the central cell, and 1×10^{11} cm^{-3} and 25 eV in the end cell without additional gas injection into D-module, respectively.

2.2. *Two-directional simultaneous photography system*

Figure 1 shows a schematic of the TDSP system (Islam *et al.* 2016; Yoshikawa *et al.* 2022) and sub-millimetre hydrogen pellet injection system (Kawamori *et al.* 2000; Kubota *et al.* 2007; Yoshikawa *et al.* 2022) installed in the central cell. The TDSP system consists of wide-angle lenses, dual branch optical fibre bundles, a TV lens and a high-speed camera (MEMRECAM GX-1, NAC Inc.). The x-direction (vertical) and y-direction (horizontal) images were observed through the horizontal side port at $z = 0$ m and on the upper side port at $z = -0.10$ m, respectively. The frame rate, imaging size and bit depth of the high-speed camera were 20 000 fps, 320×240 pixels and 8 bits, respectively. Images in the vertical and horizontal directions were obtained in the same frame of the camera system. The pixel resolution was 6.5×10^{-3} m pixel^{-1}.

2.3. *Pellet injection system*

The pellets were injected from the down side port at $z = -0.10$ m through the Teflon guide tube of 6 m from the pellet injector. The pellet injector was a pipe-gun type pneumatic pellet injector used to produce sub-millimetre pellets. The diameter and length of the pellets were controlled by adjusting the barrel size and feed gas flow rate. We used a pellet of approximately 0.7 mm in diameter and 1.8 mm in length. In the pellet diagnostic stage, two light gate systems existed for pellet velocity measurement: a microwave cavity for pellet mass measurement and a shadowgraph system for pellet form measurement. The injected fuelling pellet speed was varied from 200 to 600 m s^{-1}.

3. Tomography method for pellet ablation cloud

We used the ART for the tomography of the TDSP data of the pellet ablation cloud. ART is an iterative reconstruction technique (Guan & Gordon 1996; Zhang *et al.* 2014). It reconstructs an image from a series of angular projections, meaning that the projection

https://doi.org/10.1017/S0022377824000394 Published online by Cambridge University Press

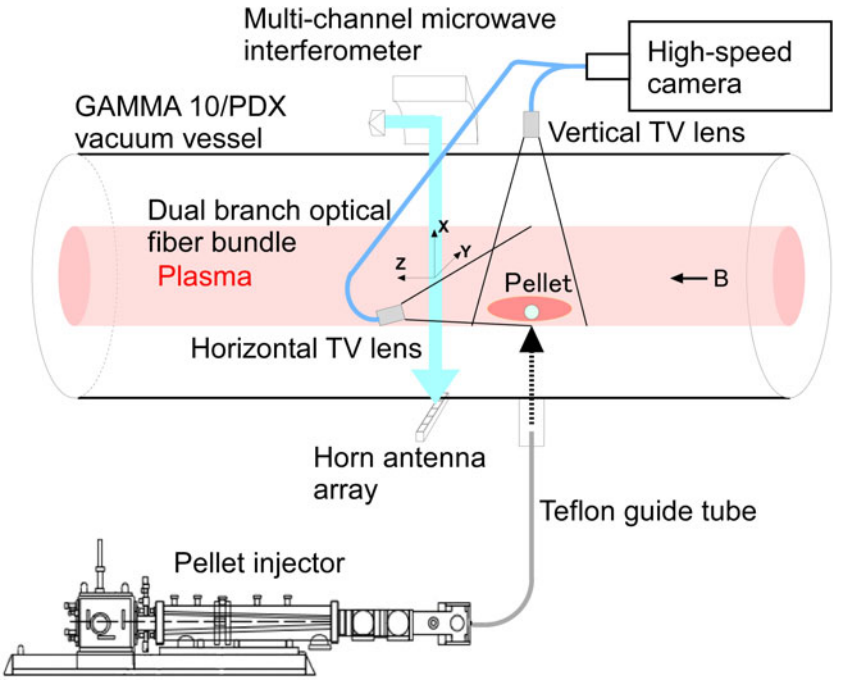

FIGURE 1. Schematic of the TDSP system, sub-millimetre hydrogen pellet injection system and multichannel microwave interferometer system in the central cell.

of image intensities along a line extends radially in the direction of a specified angle (similar to a sinogram). One advantage of the ART is that a calculation program can be constructed relatively easily with a short calculation time. For two-dimensional (2-D) iterative methods, the reconstruction problem can be formulated as a linear algebraic problem:

$$\boldsymbol{WF} = \boldsymbol{P}, \tag{3.1}$$

where $\boldsymbol{F}$ represents unknown image vector ($\boldsymbol{N} \times 1$) of $\boldsymbol{N} = n \times n$ pixels, $\boldsymbol{P}$ represents projection vector ($\boldsymbol{M} \times 1$) of $\boldsymbol{M}$ rays and $\boldsymbol{W}$ represents system matrix ($\boldsymbol{M} \times \boldsymbol{N}$) whose element w_{ij} denotes the weight coefficient representing the contribution of the jth pixel to the ith ray integral. The ART is an iterative procedure for solving (3.1). The reconstructed image elements of the jth pixel, f_j, are as follows:

$$f_j^{(k+1)} = f_j^{(k)} + \lambda \frac{p_i - \sum_{j=1}^{N} f_j^{(k)} w_{ij}}{\sum_{j=1}^{N} w_{ij}^2} w_{ij}, \quad k = 0, 1, 2, 3, \ldots, \tag{3.2}$$

where p_{i} represents the projection intensity of the ith ray, i represents $k \pmod{\boldsymbol{M}} + 1$, k denotes the number of iterations and λ denotes the relaxation parameter. In the ART method, only one sample value p_i of the projection data is used for each iteration of the image update. ART can be considered an iterative solver of a system of linear equations, where a small choice of λ results in a long iteration time but can improve the signal-to-noise ratio of the output.

https://doi.org/10.1017/S0022377824000394 Published online by Cambridge University Press

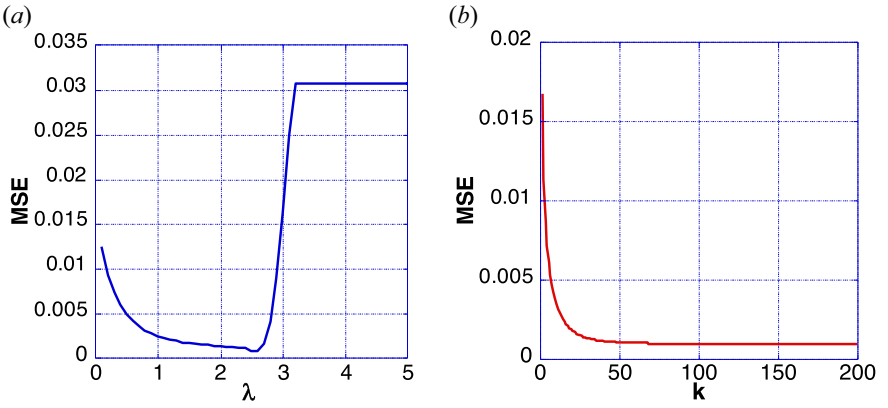

FIGURE 2. MSE against (*a*) λ and (*b*) iteration number k.

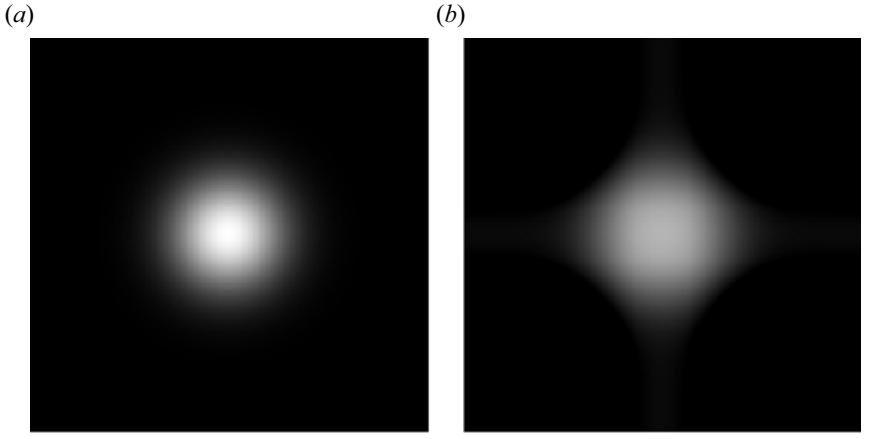

FIGURE 3. (*a*) Original image and (*b*) reconstructed image using the ART method.

3.1. *Checking the ART method*

We validated the ART method by computing image reconstructions of images that simulated pellet ablation cloud images. Figures 2(*a*) and 2(*b*) show the mean squared error (MSE) against λ with iteration $k = 100$ and iteration number k with $\lambda = 2.0$, respectively. Figures 3(*a*) and 3(*b*) show the original image of the Gaussian profile and image reconstruction using the ART method with $\lambda = 2.0$ and iteration $n = 30$. The MSE of the reconstructed image relative to that of the original image was <0.1 %.

3.2. *3-D image reconstruction*

We calculated the 2-D reconstruction images of the pellet ablation cloud in the x–y planes at each z. This implied that they were pellet ablation cloud-sliced images along the z-direction. We then obtained the pellet ablation cloud in a 3-D form by presenting the same surface images. The 3-D images reconstructed from the two-directional images are shown in figure 4. The Gaussian profiles of the two-directional images showed a spherical shape in the surface intensity at 50 % of the maximum intensity of the image.

4. Pellet injection experiments

The hydrogen plasma was produced and heated by the ion cyclotron range of the frequency wave from $t = 51$ to 440 ms and additional hydrogen gas puffing for the

https://doi.org/10.1017/S0022377824000394 Published online by Cambridge University Press

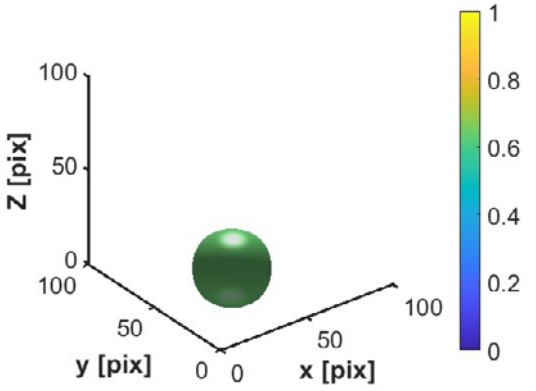

FIGURE 4. Reconstructed 3-D image.

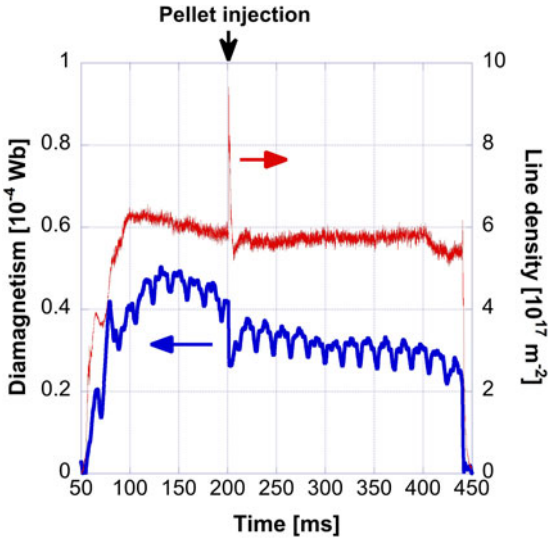

FIGURE 5. Time evolutions of diamagnetism and line density.

radiator gas in the D-module from $t = 50$ to 450 ms with a pressure of 750 mbar for the detached plasma experiment. The sub-millimetre pellet was injected into the central cell plasma at approximately $t = 200$ ms. The time evolutions of the diamagnetism and line density in the central cell are shown in figure 5, indicating the pellet injection time. Evidently, the electron line density drastically increased and diamagnetism decreased with pellet injection. Figure 6 shows the time-dependent radial profile of the electron density measured using a multichannel microwave interferometer system.

The electron density reached 7×10^{12} cm^{-3} at $t = 200.9$ ms and the plasma density peak moved from approximately $y = -2$ cm at $t = 200.5$ ms to the positive side (approximately $y = 5$ cm) at $t = 201.2$ ms.

Figure 7 shows the pellet ablation cloud images observed by the TDSP system from $t = (a)$ 200.75 ms to (l) 201.30 ms in intervals of 0.05 ms. As shown in figure 7, the vertical (left side) and horizontal (right side) wide-angle images were obtained in the same frames. The magnetic field directions and x-, y- and z-axes are shown in figure 7(a). As shown in the left-side images in figure 7, the pellet ablation clouds moved to the upper

https://doi.org/10.1017/S0022377824000394 Published online by Cambridge University Press

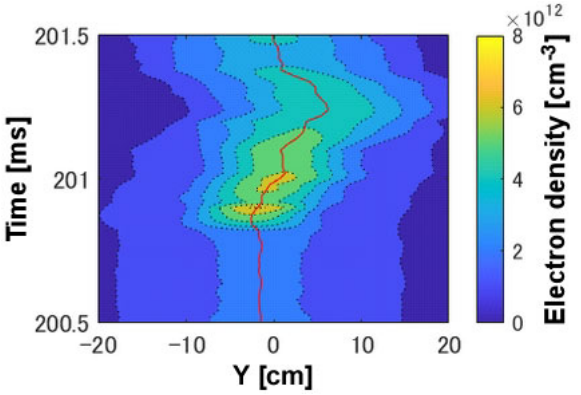

FIGURE 6. Time dependent radial profile of the electron density.

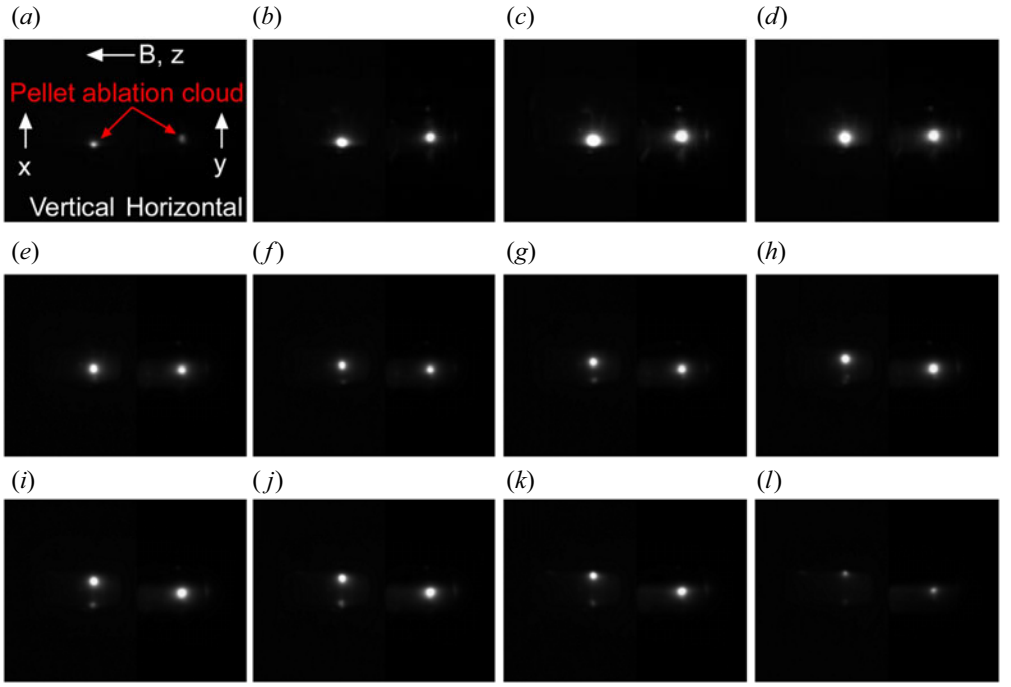

FIGURE 7. Pellet ablation cloud images measured by the TDSP from $t = (a)$ 200.75 ms to (l) 201.30 ms.

side frame-by-frame. As shown in the images on the right side, the pellet ablation clouds moved slightly from the centre of the plasma to the upper side. This result was comparable to that obtained using the multichannel interferometer system.

Figure 8 presents the 3-D reconstructed images of the pellet ablation cloud surfaces of 60 % and 55 % of maximum intensity of the images at $t = 200.80$ ms in panel (b) to 201.25 ms in panel (k), and except at $t = 201.00$ ms in panel (f), respectively. At $t = 200.75$ ms in panel (a) and 201.30 ms in panel (l), the ablation emission intensities were extremely small to show a surface intensity at 31 % and 24 %, respectively. The ablation cloud images of the surfaces used a higher intensity region in the reconstruction. This was because the image reconstructed using the ART method contained errors in the low-intensity region, such as diamond-shaped errors. This effect was eliminated from the low-intensity region.

https://doi.org/10.1017/S0022377824000394 Published online by Cambridge University Press

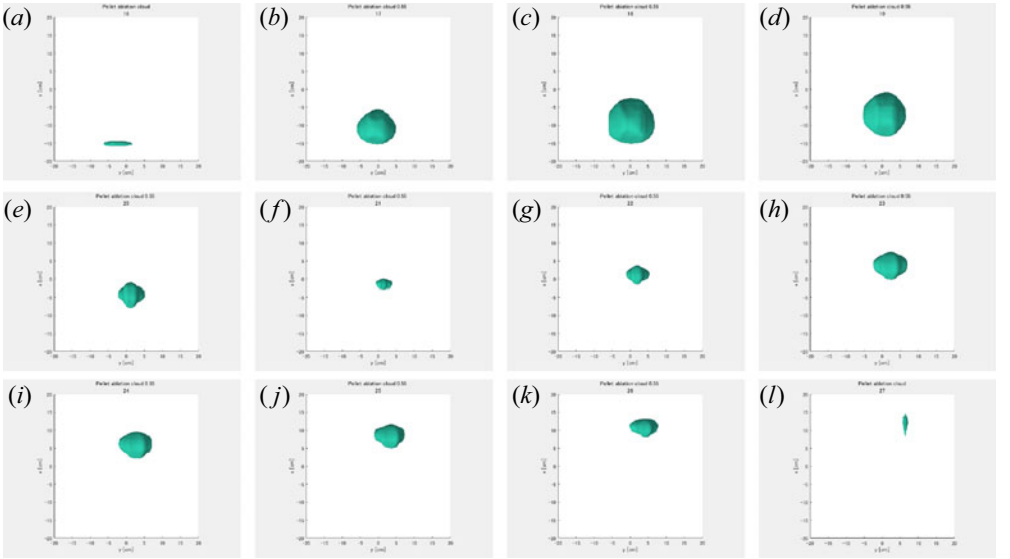

FIGURE 8. 3-D reconstructed images of pellet ablation clouds from $t =$ (*a*) 200.75 ms to (*l*) 201.25 ms.

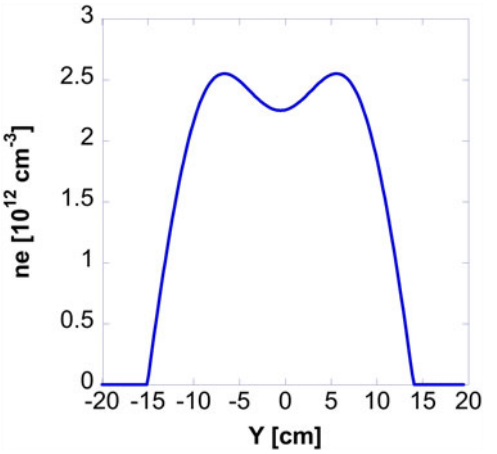

FIGURE 9. Electron density radial profile before pellet injection.

5. Discussion

The form of the pellet ablation cloud had the largest spherical shape at approximately $x = -8$ cm and the smallest oval shape at approximately $x = 0$ cm. On the upper side of the plasma, the pellet ablation cloud size was large at approximately $x = +8$ cm; this was the same as that on the lower side. The larger pellet ablation cloud size at approximately $x = -8$ and $+8$ cm was due to the radial profile of the hollow plasma density. Figure 9 shows the electron density radial profile before the pellet injection. The electron density radial profile was hollow. Pellet ablation strongly depends on the plasma density.

The pellet completely penetrated the plasma. Figures 10(*a*) and 10(*b*) show the pellet ablation cloud motion obtained from the centroids of the 3-D reconstructed images in the *x*–*y* and *x*–*z* planes. The error bars show the radius of the pellet ablation cloud surfaces. Pellet ablation clouds moved from approximately $x = -13$ cm to 12 cm, approximately

https://doi.org/10.1017/S0022377824000394 Published online by Cambridge University Press

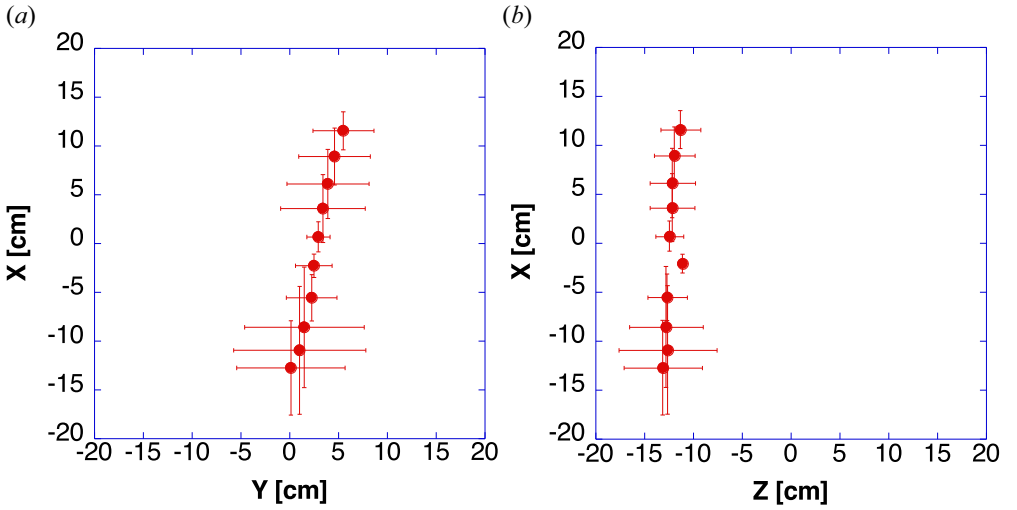

FIGURE 10. Pellet ablation cloud motion obtained from the centroids of the 3-D reconstructed images. Error bars show the radius of pellet ablation cloud surfaces.

$y = 0$ cm to $+6$ cm and approximately $z = 13$ cm to -10 cm. The pellet ablation cloud z position at $t = 200.95$ ms deviated from the other positions. The reason for this is unclear; however, the deviation was in the reconstructed resolution of approximately 1 cm. The pellet crossing speed in the plasma was approximately 6×10^2 m s^{-1}. The pellets moved diagonally across the plasma. The motion of the pellet ablation cloud was almost the same as the peak motion of the electron density (red line in figure 6). The electron density was strongly affected by the pellet ablation cloud motion. The electron density peak at $t = 200.9$ ms had a large amount of fuelling source from the pellet injection, as observed in the large pellet ablation cloud image in figure 8(*c*). We successfully obtained pellet ablation clouds in 3-D images and determined their behaviour in plasma for the first time.

6. Conclusion

We observed the pellet ablation cloud and its trajectory in the plasma using the TDSP system in a GAMMA 10/PDX pellet injection experiment and successfully obtained 3-D images and determined their 3-D behaviour for the first time. The pellet ablation cloud motion and image surface size were strongly correlated with the electron density peak position and electron density increase.

Acknowledgements

The authors sincerely thank the members of the GAMMA 10 group for their collaboration in the experiments.

Editor Cary Forest thanks the referees for their advice in evaluating this paper.

Funding

This study was supported by the bilateral collaboration research program in the University of Tsukuba and Kyoto University (NIFS20KUGM148, NIFS20KUGM159, NIFS21KUGM165 and NIFS21KUHL101).

Declaration of interests

The authors report no conflict of interest.

Data availability statement

The data that support the findings of this study are available from the corresponding author upon reasonable request.

REFERENCES

BALDZUHN, J., *et al.* 2019 Pellet fueling experiments in Wendelstein 7-X. *Plasma Phys. Control. Fusion* **61**, 095012.

BAYLOR, L.R., MEITNER, S.J., GEBHART, T.E., CAUGHMAN, J.B.O., SHIRAKI, D., WILSON, J.R., CRAVEN, D., FORTUNE, M., SILBURN, S., MUIR, A., PEACOCK, A.T., PARK, S.H., KIM, K.P., KIM, J.H., LEE, K.S., ELLWOOD, G., JACHMICH, S., KRUEZI, U., LEHNEN, M. & JET CONTRIBUTORS 2021 Design and performance of shattered pellet injection systems for JET and KSTAR disruption mitigation research in support of ITER. *Nucl. Fusion* **61**, 106001.

COMBS, S.K., MILORA, S.L., BAYLOR, L.R., FOUST, C.R., GETHERS, F.E. & SPARKS, D.O. 1985 A three-barrel repeating pneumatic pellet injector for plasma fueling of the Joint European Torus. *Rev. Sci. Instrum.* **56**, 1173.

GUAN, H. & GORDON, R. 1996 Computed tomography using algebraic reconstruction techniques (ARTs) with different projection access schemes: a comparison study under practical situations. *Phys. Med. Biol.* **41**, 1727.

ISLAM, M.M., NAKASHIMA, Y., KOBAYASHI, S., NISHINO, N., NAKANO, Y., HOSOI, K., ICHIMURA, K., ISLAM, M.S., SHIMIZU, K., FUKUI, K., OHUCHI, M., TERAKADO, A., YOSHIKAWA, M., KOHAGURA, J., HIRATA, M., IKEZOE, R., WANG, X., ICHIMURA, M., SAKAMOTO, M. & IMAI, T. 2016 Effect of laval nozzle in the GAMMA 10 SMBI experiments. *Plasma Fusion Res.* **11**, 2402053.

KAWAMORI, E., TAMANO, T., NAKASHIMA, Y., YOSHIKAWA, M., KOBAYASHI, S., CHO, T., ISHII, K., MASE, A. & YATSU, K. 2000 Preliminary pellet injection experiment in the GAMMA 10 tandem mirror. *Plasma Fusion Res. Ser.* **3**, 473.

KUBOTA, Y., YOSHIKAWA, M., NAKASHIMA, Y., KOBAYASHI, T., HIGASHIZONO, Y., MATAMA, K., NOTO, M. & CHO, T. 2007 Behavior of hydrogen fueled by pellet injection in the GAMMA 10 tandem mirror. *Plasma Fusion Res.* **2**, S1057.

NAKASHIMA, Y., *et al.* 2015 Progress of divertor simulation research toward the realization of detached plasma using a large tandem mirror device. *J. Nucl. Mater.* **463**, 537.

SAKAMOTO, R., YAMADA, H., TANAKA, K., TOKUZAWA, T., MURAKAMI, S., GOTO, M., MORITA, S., OHYABU, N., KAWAHATA, K., MOTOJIMA, O. & EXPERIMENTAL GROUP, L.H.D. 2004 Observation of pellet ablation behaviour on the large helical device. *Nucl. Fusion* **44**, 624.

YOSHIKAWA, M., *et al.* 2021 Study of detached plasma profile in the divertor simulation experimental module of tandem mirror GAMMA 10/PDX. *AIP Adv.* **11**, 125231.

YOSHIKAWA, M., KOHAGURA, J., CHIKATSU, M., SHIMA, Y., SAKAMOTO, M., NAKASHIMA, Y., MINAMI, R., YAMADA, I., YASUHARA, R., FUNABA, H., MINAMI, T. & KENMOCHI, N. 2018 Radial profile measurements of electron temperature and density using the thomson scattering system in GAMMA 10/PDX. *Plasma Fusion Res.* **13**, 3402051.

YOSHIKAWA, M., NAKASHIMA, Y., KOHAGURA, J., SHIMA, Y., NAKANISHI, H., TAKEDA, Y., KOBAYASHI, S., MINAMI, R., EZUMI, N. & SAKAMOTO, M. 2022 First observation of pellet ablation clouds using two-directional simultaneous photography in GAMMA 10/PDX. *Plasma Fusion Res.* **17**, 1202093.

ZHANG, S., ZHANG, D., GONG, H., GHASEMLIZADEH, O., WANG, G. & CAO, G. 2014 Fast and accurate computation of system matrix for area integral model-based algebraic reconstruction technique. *Opt. Engng* **53**, 113101.

https://doi.org/10.1017/S0022377824000394 Published online by Cambridge University Press